Pore-Pressure-Dependent Performance of Rocking Foundations

Arash Esmatkhah Irani[1], Masoud Hajialilue-Bonab[2], Arya Assadi-Langroudi[3,*], Emad Maleki Tabrizi[4]

[1] Research Associate, Emerging Geohazards laboratory, University of East London; arash.esm.ir@gmail.com

[2] Professor, Civil Engineering Department, University of Tabriz; Tabriz 5166616471, hajialilue@tabrizu.ac.ir

[3] Associate Professor, Emerging Geohazards laboratory, University of East London; 4-6 University Way, London E16 2RD; A.Assadilangroudi@uel.ac.uk (Corresponding Author)

[4] Graduate MSc, Civil Engineering Department, University of Tabriz; Tabriz 5166616471, emad.malekitabrizi@gmail.com

Notion List

A	Area of the footing
A_c	Minimum soil-footing contact area
α	Amplification
B	Width of the footing
D_w	Depth of water
D_r	Relative density
D_s	Depth of failure wedge
Δ	Horizontal distance between the centre of gravity and mid-foundation
Δu	Pore water pressure
f	Frequency of input motion
$f_{n,i}$	Frequency at time instant i
h_{cg}	Distance from the footing base
K_r	Rotation stiffness
M	Mass
$M_{c,foot}$	The foundation theoretical ultimate moment capacity
L	Length of the footing
L_c	Critical length

PGA	Peak ground acceleration
r_s	Sphericity
r_r	Roundness
S	Degree of saturation
ξ	Damping ratio
ξ_i	Damping ratio at time instant i
$T_{n,i}$	Period at time instant i
θ_f	Rotation of footing
w_{sat}	Saturated water content
ω_n	Natural frequency of oscillation

Abstract

This study explores the concept of rocking foundations to mitigate damage during seismic events. By weakening the footing intentionally, the foundation acts as a "fuse" to prevent plastic hinges from forming in columns. Shake table experiments were conducted on a lightweight prototype deck mass-column-footing model founded on a fine, medium-dense sand, in two states of nearly dry and saturated. Kinetic energy dissipation, hysteresis, and decay are examined for various structure masses, for two nominal low and high motion frequencies. Findings suggest that energy dissipation is higher in saturated sands — as compared to nearly dry and despite the absence of liquefaction — due to fluctuating pore water pressure and a suction effect that evolves beneath foundations' edge. Where the substrate retains its original porosity, flow of water and subsequent damping becomes pivotal mechanisms to enable the rocking motion. In dry sands, energy dissipation occurs mainly through rotation, and enhances with motion frequency (from testing 3 to 5 Hz). In saturated sands, energy dissipation occurs predominantly through plastic settlement, and becomes less effective with motion frequency. Lighter structures experience greater rotational movement, especially in the case of dry sands. That enhanced rotational movement is drove by lower rotational stiffness. Overall, lighter structures facilitate the re-centring of the foundation upon rocking motion.

Key words

Rocking; Rotation; Settlement; Saturation; Mass; Frequency; Damping

INTRODUCTION

The recommended response for foundations, as per current geotechnical codes of practice (e.g., EC8), remains to be elastic [1]. Conventional foundations are fixed base [2] and allow ductile plastic hinging to form at the base of the column. However, an inelastic soil-footing response under seismic shaking is inevitable and the consequent non-linear soil-structure interaction can become beneficial in design. Seismic isolation through rocking motion is a relatively recent design approach that provides seismic resilience by allowing subgrade soil to locally fail and enter the non-linear plastic range of strains [3,4]. Foundation rapidly reaches its ultimate capacity, rotates back and forth, and minimises the inertia forces that otherwise would transmit onto the structure.

In nature, the rocking effect resembles how tumbleweed responds to multilateral forces and moments. Tumbleweeds are detached from their roots and can rotate on their toes, lift, settle back down, and roll in windy weather. Fig. 1(a) shows the movement of a tumbleweed. Fig. 1(b) illustrates the rotations that cause the rocking foundation effect. The gravitational forces and breakaway gaps enable the system to restore the vertical orientation [5].

Seismic isolation

Rocking foundation as a concept was first introduced by Housner [6]. The concept incorporates weakening at the base through decreasing footing length or reinforcements. Consequently, the foundation theoretical ultimate moment capacity ($M_{c,foot}$) is decreased, transforming the foundation into a “fuse” to avoid plastic hinges forming in the column. The weakening naturally leads to a small factor of safety (2 to 8) for the vertical bearing pressure which then costs excessive foundation settlements [7]. Such movements necessitates incorporation of performance-based seismic design (PBSD), albeit PBSD in the rocking foundation context remains to be much further studied [8]. Countermeasures include the placement of reaction blocks and concrete pads around the foundation edges [9] piles and stone columns in softer soils [10]. The moment capacity ($M_{c,foot}$) is the primary factor that determines the energy dissipation. Gajan and Kutter [11] formulated the moment capacity as a function of vertical load applied to the centre of gravity (P, applied at a h_{cg} distance from the base), and the rocking re-centring distance (Δ, horizontal distance between the centre of gravity and middle of soil-footing reduced contact area). The Δ is associated with the contact area between the soil and the foundation, and how it evolves during the motion. To this end,

$$M_{c,foot} = P\Delta = \frac{PL}{2}\left(1 - \frac{A_c}{A}\right) \tag{1}$$

where A_c is the critical contact area needed to carry the vertical load of structure, thereby dependent on factor of safety. In Fig. 1(b), L_c is the critical length, or the soil-footing contact length over which the bearing pressure becomes equal to the ultimate bearing resistance as defined by Terzaghi [12]. The L_c is the minimum length of footing-soil interface as foundation rocks. In Eq. 1, L is the length of footing along the direction of motion, and A is the footing area.

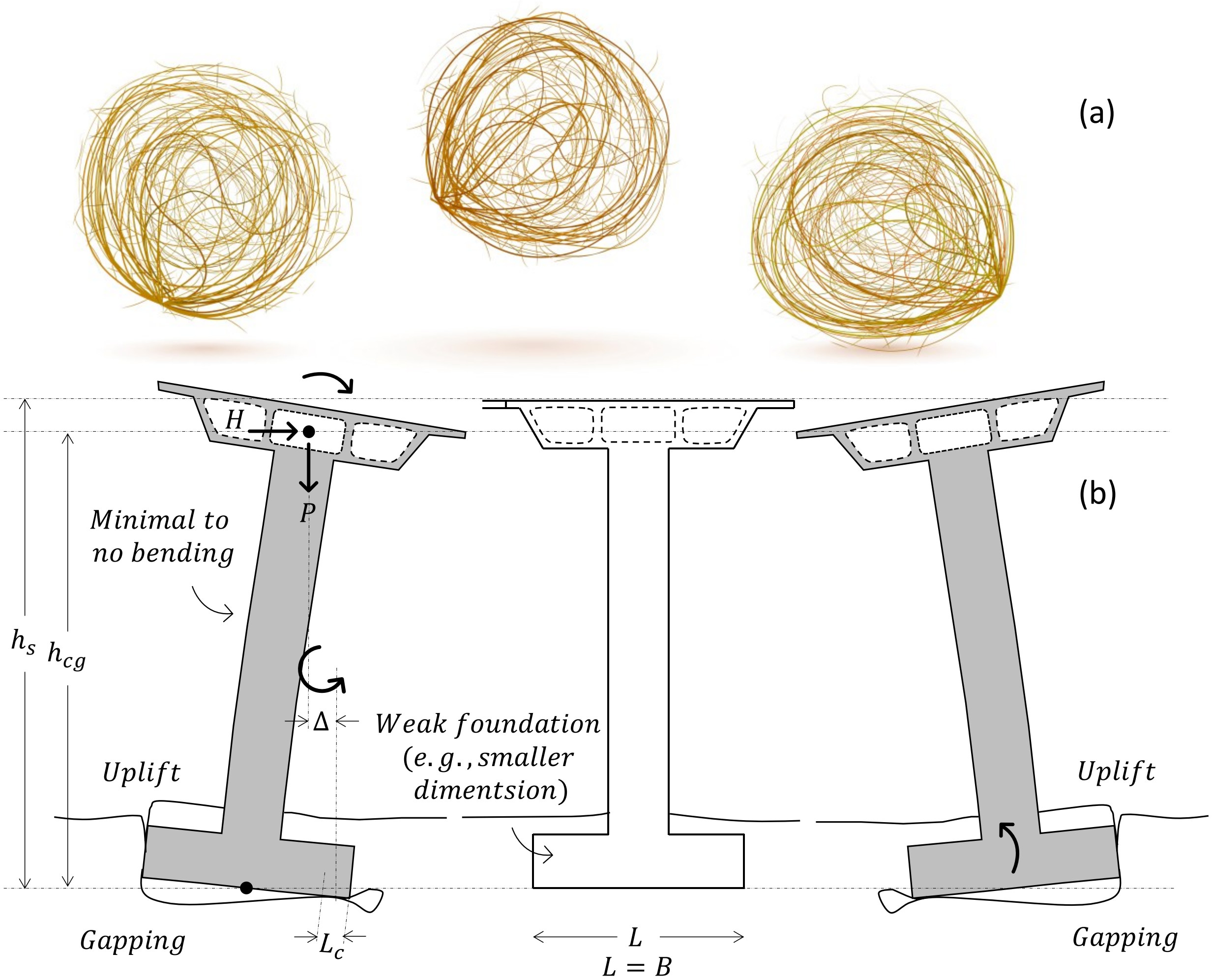

Fig. 1. Fuse mechanism: (a) tumbleweed plant detached from root and its survival from wind effect through movement and minimised ductility demand (Adobe Stock #449307469, licence AE02295300753CGB); (b) rocking motion as plastic hinge develops at soil-footing interface.

The predominant assumption is that foundations can rock when weakened, and that rocking takes place on homogeneous sands [13] that are fully saturated, dense, and well compacted [14]. Note that rocking is also a mechanism in clayey, cohesive soils, although it has been comparatively less studied. The PhD work of Hakhamaneshi [15] is a seminal contribution in this area. Their research showed that plastic settlements in clay are 20 to 40% less than typical settlements in sand under similar critical contact area ratios and rotation demands. They also linked the phenomena of breakaway gaps and uplift, as observed in rocking foundations, to those on sandy soils. Sharma and Deng [16] referred to field snap-back trials and demonstrated a "better than on sand" recentring capability of rocking foundations on clays (see also Sharma and Deng [17]).

In much of the previous literature, shallow foundations are also assumed to rest either at the surface or with minimal embedment [23]. Sand is mostly considered dry [7, 11, 18, 19, 20] or saturated [14, 20, 21, 22]. Groundwater level however fluctuates, leading to changes in the degree of saturation of the subgrade soil. The impact of such variations has not received equal attention. Burland and Burbidge [24] investigated the effect of the water table on foundation settlement and constrained that association to a marginal 13% (in total settlement) for sands. Nevertheless, they emphasized on the more significant overall effect on the ultimate bearing capacity. Under seismic conditions, the water table influences the settlement, rotation, overturning moment, and energy dissipation characteristics of rocking foundation systems [25]. The rocking foundation response for unsaturated soils is not an objective in this paper, but this is an interesting, rapidly growing field of study. Immediate expectations from unsaturated soils, when compared to their dry and saturated state are an increase in soil stiffness and moment capacity, lower damping, and lower foundation seismic settlement, and rotation at the surface [16, 23].

This paper presents the findings from experiments conducted on a model surface shallow foundation founded on a medium dense sand in two states of nearly dry and fully saturated. Resting on sand were four lightweight model columns and decks with a 0.04 scale factor. Mass was varied. A 1-g shake table was used to model a 0.2 g peak ground acceleration (PGA) earthquake at two, nominally low and high, 3 and 5 Hz frequencies to study the evolution of pore water pressure, energy (acceleration) dissipation, stiffness degradation, and displacements beneath foundation.

Principles behind the fuse mechanism, design of the physical model, observations, and analysis are presented in the following sections.

EXPERIMENTAL PROCEDURES

Design principles

A mid-rise lightweight prototype deck mass-column-footing model was designed based on a fixed-base 1.82-m diameter 11-m high column on Iranian standard F161 sand. Four design criteria were followed:

(a) the system was a single-degree-of-freedom model with length scale factor of 0.04;

(b) the system was designed for a nominally elastic response of the column;

(c) a moment-to-shear ratio of $h_{cg}/\mathrm{B} = 3$ was adopted, where h_{cg} is the height from the base of the footing to the centre of gravity of the seismic mass and B is the length of the footing in the direction of shaking. Theoretically, a $h_{cg}/B > 1$ moment-to-shear ratio encourages rocking motion instead of translational movements;

(d) The critical contact area ratio, A/A_c, of the footing ranged from 1.81 to 2.69 regardless of the soil saturation conditions. Here, A is the initial soil-footing contact area and A_c is the minimum soil-footing contact area that supports the vertical load during rocking. The A_c was determined in correspondence with method proposed by Deng and Kutter [26] and the Brinch Hanson bearing capacity equations [27]. In Fig. 1(b), $L_c = A_c/B$.

Generally, in reduced-scale physical modelling, accurately reproducing stress fields within the soil is challenging due to scale effects. These effects arise because the behaviour of soil under load is pressure-dependent, which means that the smaller scale of the model may not perfectly mimic the actual stress conditions in a full-scale scenario. The length scale factor of $\lambda = 0.04$ adopted here means every 1 metre in the model represents 25 meters in the prototype. Despite the factor, the constrained depth of the soil layer inevitably leads to different interaction dynamics between the foundation and the soil compared to a full-scale model where soil depth might be more extensive. This includes potential differences in how the soil densifies or how stress is distributed through the soil column during seismic events.

Design principles led to a system with properties summarized in Table 1.

Table 1 Model properties in scaled dimensions

Property	Value
Moment-to-shear ratio, $h_{cg}/$B	3
Critical length, L_c: m	0.085 - 0.129 †
Critical contact area ratio, A/A_c	1.81 - 2.69 †
D_w/B	0.26 ‡

† Depending on mass of structure

‡ D_w is depth of water above pore water pressure transducers, B is footing width in the direction of shaking

Model structure

A 3000×2000 mm ($L \times B$), indoor, one-dimensional shake table with 6 tonnes ultimate load capacity and ±100 mm horizontal displacement range was used to generate uniaxial excitation (see Fig. 2(a) and (b)). The table was designed and fabricated at Tabriz University. The foundation soil was contained in a $650 \times 1000 \times 600\ mm$ $(L \times B \times H)$ rigid box composed of clear and stiff PMMA panels and an exterior steel support frame. From bottom, the box was lined with a layer of gravel which was in receipt of water through two tubes connected to drainage valves installed on the box sidewalls. A protective nonwoven geotextile layer covered the gravel and extended along the sides of the box. The rigid box was loaded onto the shake table using a crane (Fig. 2(c)) and subsequently bolted to the shake table base (Fig. 2(d)). Model footing was square in shape and 230 mm in width, resting on surface and above the subgrade sand. The footing was connected to a $230 \times 230 \times 82$ mm rigid steel plate (i.e., load stub) via a 76.2-mm-diameter tubular column (Fig. 2(e)). The load stub provided seating space for four mass blocks (20, 25, 30 and 60 kg). The total mass of footing, column and load stud equalled 19.26 kg. The h_{cg} was set at 438 mm.

Fig. 2. Experimental set up: (a) shake table; (b) hydraulic actuator connected to control system; (c) installation of box on shake table; (d) and (e) deck mass-column-footing model.

Soil material

The foundation soil was a well-sorted ($C_u = 1.87$), fine (0.80 to 1.18 mm, and a $D_{50} = 0.27$ mm), and sub-angular ($r_s = 0.60$, $r_r = 0.38$) sand, similar to standard Ottawa C109 Sand in size and shape. The sand is commercially available under F161 brand name and has a specific gravity of $G_s = 2.65$, maximum void ratio of $e_{max} = 0.815$ and minimum void ratio of $e_{min} = 0.534$. Two sand conditions were examined: fully saturated and nearly dry. Sand was loaded into the box in loose lifts and compacted with a hand-held vibratory compactor and a $580 \times 410 \times 50$ mm plate, into 50 mm thick layers to achieve a target relative density of 75%. Compaction water content varied between 2 to 5 wt.%. Based on the results of sand cone tests, conducted in various stages of construction, the achieved mean relative density was 72.3%, corresponding to a void ratio of 0.74, bulk unit weight of $\gamma = 15.71$ kN/m³ and a degree of saturation between 7.2 and 17.9%. The peak drained angle of friction for sand was 33° based on direct shear test results. For saturated models, water was introduced to compacted soil in the box from two ports on sidewalls of box, and through tubes that extend into the gravel layer. Valves were closed when water table raised about 50 mm above soil surface. In saturated state, soil had a bulk unit weight of $\gamma = 19.12$ kN/m³ and a saturated water content of $w_{sat} = 27.8\%$.

Instrumentation

An array of 10 sensors, including five 0.01g in precision accelerometers (Acc), 2 linear variable differential transformers (LVDTs), three 50-kPa in capacity pore water pressure transducers and two cameras (for control) were utilised in experiments. Figure 3 shows a schematic front elevation view of the model and the instrumentation layout. One accelerometer was placed at the shake table platen (Acc5), one on the mass block (Acc4), and three within the subgrade soil. Pore pressure transducers were installed within the wedge of failure (also known as zone of shear and depth of the rocking foundation) below the edges of the foundation and at a proximity. Rocking motion takes place within this wedge, with depth of about $D_s = 0.5L_c.tan(45 + \emptyset'/2)$ — this is approximately 20 mm in the present study. LVDTs were installed aligned with the direction of seismic motion. Two cameras were used to capture videos of test sequence.

Testing diet

The test protocol included sinusoidal signals. Acceleration time histories are presented in Fig. 4(a) and (b). In total, 16 shake table experiments were performed: 8 experiments on nearly dry sand, constituting two motion frequencies of 3 and 5 Hz and four concentrated masses. Experiments were repeated for saturated sand.

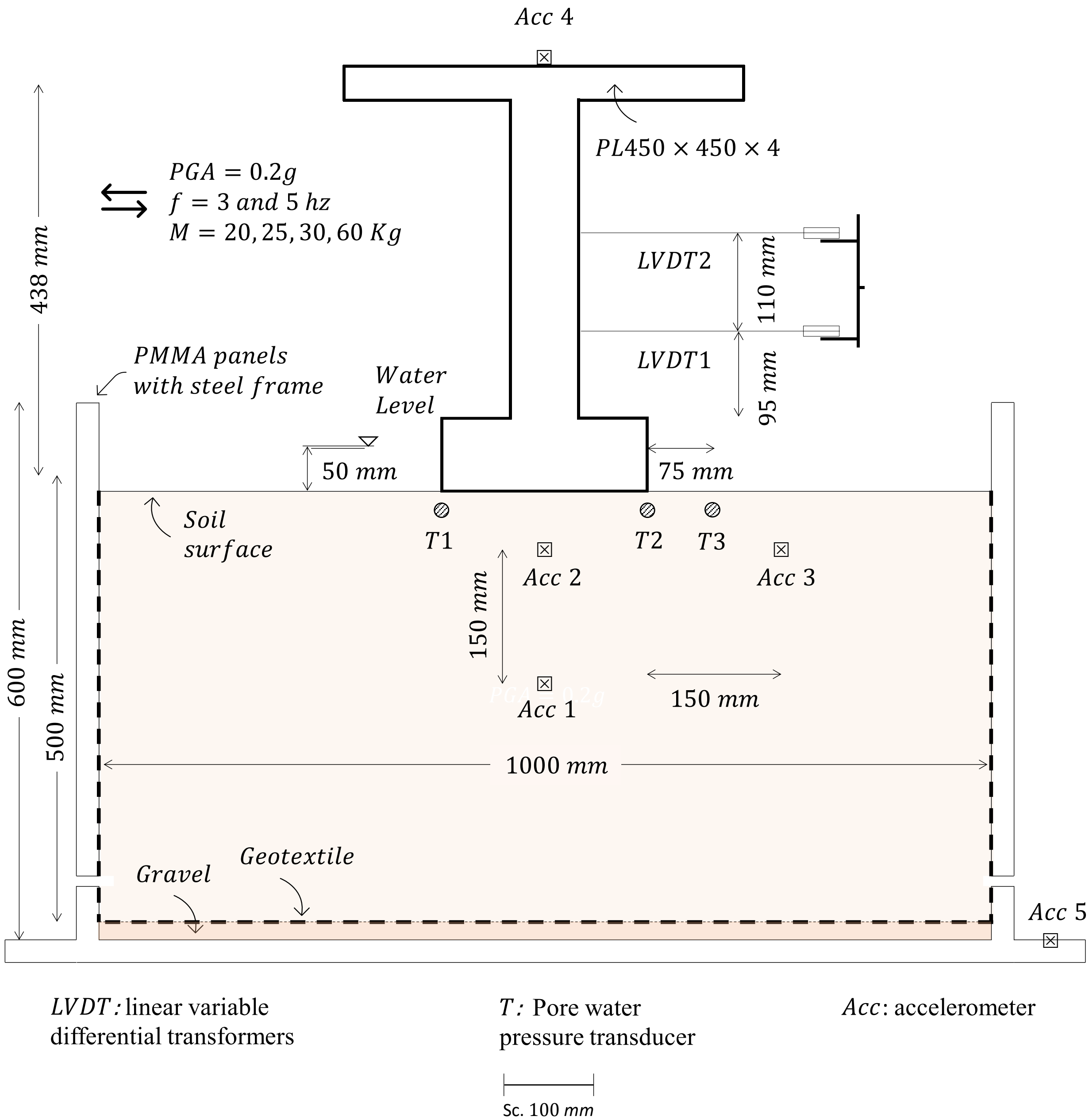

Fig. 3. Schematic diagram of the physical model and the instrumentation layout

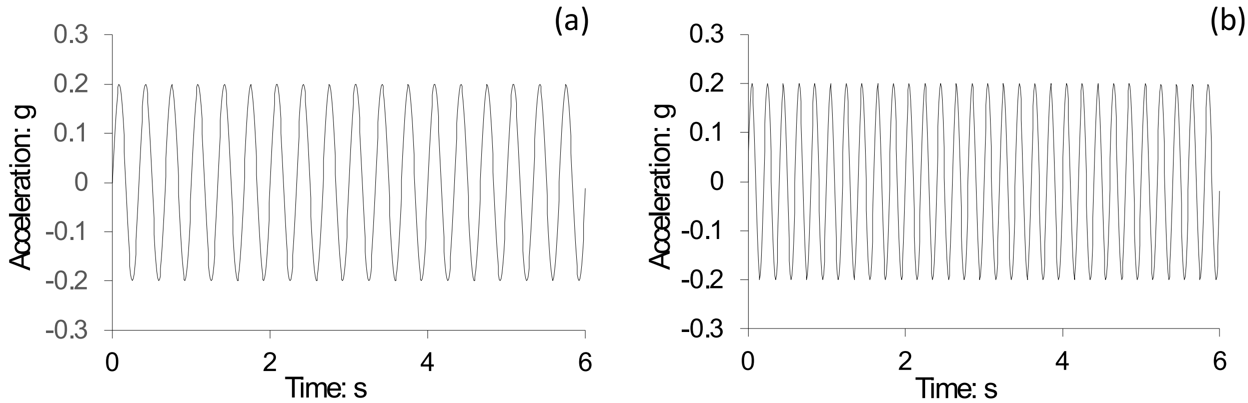

Fig. 4. Acceleration time histories for input signal: (a) $f = 3$ Hz, (b) $f = 5$ Hz.

ENERGY DISSIPATION

From Amplification Perspective

In general, greater energy dissipation in a substrate during vibration can be indicated by two readings. Firstly, evidence in support of reduced peak acceleration: If the peak accelerations are lower, one may conclude that the energy introduced by the vibration dissipates more within the medium. Secondly, evidence for increased damping characteristics: This can be observed if the vibrations die down more quickly, meaning the acceleration returns to zero faster.

Figure 5 illustrates a set of acceleration time history graphs, divided into two main categories based on their location: beneath the foundation centre and at the top of the structure. Each set includes four diagrams. Figs. 5(a), 5(b), 5(c) and 5(d) represent the acceleration measured by Acc2, beneath the foundation centre. Figs. 5(e), 5(f), 5(g) and 5(h) illustrate the acceleration measured by Acc4, at the top of the structure — that is near the centroid of the deck. Measurements were constrained to two motion frequencies of 3 and 5 Hz. The case of saturated sand indicates lower peak accelerations beneath and above the structure. The dissipation appears to be relatively more rapid for systems subjected to higher frequency motion of 5 Hz.

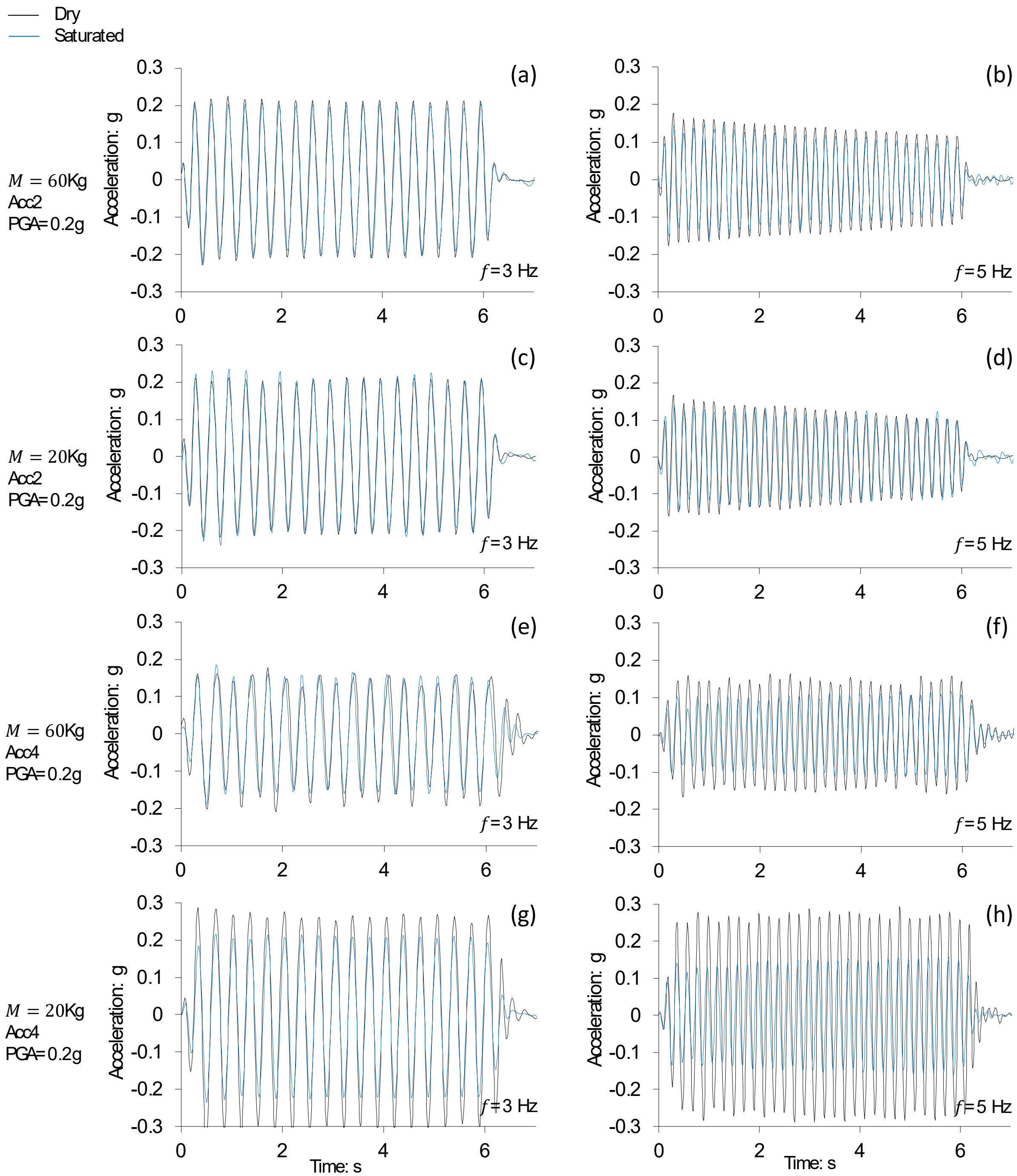

Fig. 5. Acceleration time histories for (a), (b), (c) and (d): beneath the footing's centre; (e), (f), (g), (h): top of the structure.

The more marked energy dissipation in the case of saturated sand can be, partly, attributed to the relatively greater damping ratio.

Mechanisms

It will be shown, in Fig. 6, that motion generates an excess pore water pressure in saturated sand. It will be also discussed that, motion-induced pore water pressure causes an array of vertical displacements including formation of a breakaway gap. The latter enables the rotation, rocking, thereby rapid fluctuations of pore water pressure across negative and positive values. As motion matures, the pore water pressure subsides from its initial high due to gradual expulsion of water from the soil network of pores. The substantial settlements in the case of saturated sand — see Figs. 8(a)-(d), is consistent with effects of progressive water expulsion. The efflux of water is not immediate despite the fundamentally drained nature of medium dense sand. In particular, in regions close the centre (and below) of the foundation, the offset from drain points delays the outflow of water. The flow of pore water to drain points creates internal friction within the sand, leading to partial dissipation of energy. The measured lower amplifications (see Fig. 5) in saturated sand is due to the latter damping effect. It is also evident that the ground motion amplification modestly decreases with motion time, particularly at higher 5 Hz frequency. The decrease is, by-and-large, more pronounced in saturated sand. This progressive loss of amplification lends further evidence to greater damping in saturated sands. Figs. 5(e) and (f) illustrate the registered acceleration on top of the structure. As of the substrate, lower amplification was registered in structures on saturated sand.

From Pore Pressure Perspective

Figs. 6(a)-(b) show the variation of pore water pressure over time beneath the foundation. In Fig. 6(a), the rotational rocking motion is evident from the differences in pore pressures beneath the edge of the footing (T2) compared to points further away from the edge, yet still near the foundation (T3).

In principle, a registered positive pressure coincides with settlement, and a negative pressure with uplift movement. During motion and for saturated sand, motion generates an immediate excess pore water pressure, a drop in effective stress and a consequent buoyancy force with a tendency to lift the foundation. The uplift causes a breakaway gap beneath the foundation, and consequently development of negative pore water pressure. The negative pressures create a suction effect that facilitate both movement of fluids and re-centring of the foundation. In Fig. 6(a), negative pressure appears to be more marked under the edge of the footing (T2) and retains amplitude for the entire motion duration (i.e., 6 seconds). As such, for any structure mass, it appears that the breakaway gap remains open to enable water influx and efflux. In contrast, the negative pressure decreases with motion time in surrounding areas (see T3). Upon termination of motion, pore pressures tremble within a positive range of values before returning to hydrostatic levels. This indicates post-excitation expulsion of water, densification of soil (i.e., consolidation), and ground settlement. Note the presence of positive pore pressures (on termination of the vibration) leads to plastic settlements after dynamic motion. This will be further discussed in following sections.

Fig. 6(b) illustrates the variation of pore water pressure with time beneath the edge of the footing and for two concentrated masses of 20 and 60 kg. Beneath the edge of the footing and under the lightest structure (20 kg), for the select motion time range of 4.2 to 6.2 s, Figs. 6(c) and 6(e) show the variation of motion acceleration and pore water pressure respectively. Figure 6(d) and 6(f) show similar diagrams for the edge of the footing under the heaviest structure (60 kg). Beneath the lightest structure (20 kg) and edge of footing, pore water pressure appears to tremble more frequently. This is a manifestation of relatively easier re-centring and can be explained from two perspectives. Firstly, the relatively more porous subgrade soil beneath the lighter structure provides sufficient space for pore water to mobilize. The short wavelength cycles in Fig. 6(e) may be attributed to that greater porosity. Secondly, the relatively more permeable substrate beneath the lighter structure facilitates formation of the breakaway gap, which then accommodates the mobilized water and causes the tremors seen in Fig. 6(e). The gap is an enabler for the rocking motion. The amplification beyond the input $\alpha = 0.2$ g on top of the structure in Fig. 5(g) and 5(h) is consistent with this enhanced rotation. In Fig. 7, the range of footing rotation angles increase with decreasing structure mass. In other words, lighter structures benefit from a breakaway gap to experience greater levels of footing rotation. Regardless of structure mass, negative pore water pressures retain amplitude for the entire motion duration.

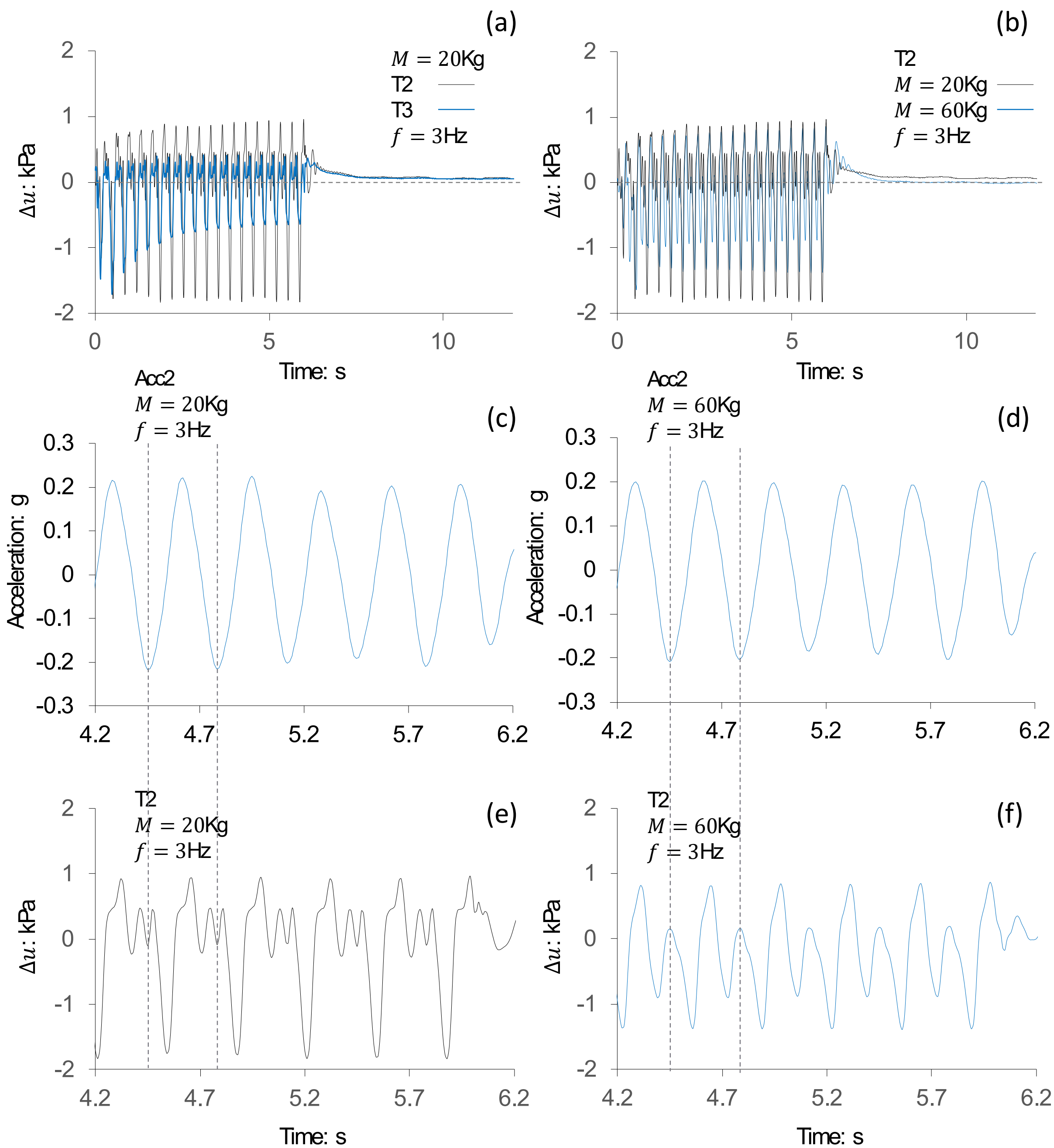

Fig. 6. Saturated sand profiles (a) pore water pressure evolution beneath the footing's edge (T2) and proximity (T3); (b) pore water pressure evolution beneath the edge of footing for varied surcharge; (c) and (e): acceleration and pore pressure evolution beneath the footing – light structure; (d) and (f): acceleration and pore pressure evolution beneath the footing – heavy structure.

ROCKING RESPONSE

Hysteresis Response

Fig. 7 exhibits normalised overturning foundation moment versus rotation in the direction of input motion (θ_f) for nearly dry and saturated conditions. De-centralised and modestly wider hysteresis loops for saturated sands indicate enhanced levels of damping and energy dissipation. This is consistent with acceleration time histories observed in Fig. 5.

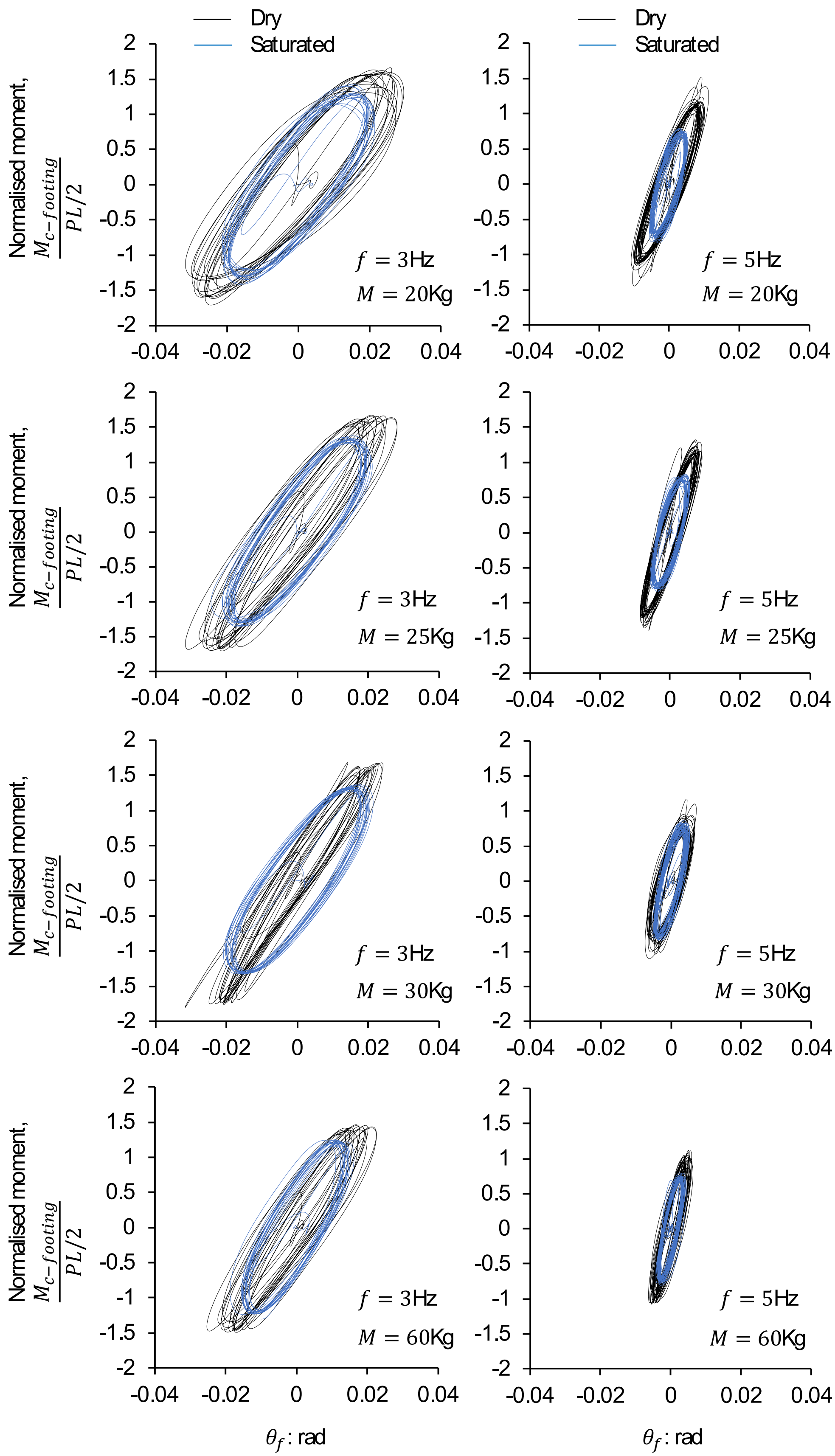
Dry
Saturated
Normalised moment, $\frac{M_{c-footing}}{PL/2}$
f = 3Hz
M = 20Kg
f = 5Hz
M = 20Kg
f = 3Hz
M = 25Kg
f = 5Hz
M = 25Kg
f = 3Hz
M = 30Kg
f = 5Hz
M = 30Kg
f = 3Hz
M = 60Kg
f = 5Hz
M = 60Kg
θ_f: rad

Fig. 7. Normalised moment-rotation hysteresis loops

Irrespective of motion frequency and mass, saturated sands generally exhibit lower peak moment and peak rotation (also see Antonellis et al. [28] and Turner et al. [25]). The response seems to be influenced by factors such as the initial packing quality, applied vertical load, and embedment depth. In this study, the subgrade sand used is relatively more porous (D_r of around 72%), supports relatively lighter masses, and underlies a surface footing without any embedment. To this end, although the nearly dry sand develops some apparent cohesion (through matric suction) to arrest rotation, the cohesion and subsequent restrictions to motion are strictly limited. In Fig. 7, the hysteresis loops for nearly dry sand close with increasing structure mass, indicating a reduction in energy dissipation. The motion results in a greater degree of densification of subgrade soil beneath the heavier structure, a reduction pore space size and, consequently, an increase in matric suction when conditions favour its development.

Total Kinetic Energy

For the mass-pier-foundation system subjected to dynamic excitation, the total kinetic energy constitutes the kinetic rotation energy and the kinetic translational energy. The kinetic rotation energy is equal to the contained area in each hysteresis loop. The kinetic translational energy is a factor of foundation settlement.

In Fig. 7, the nearly dry sand exhibits a much larger hysteresis area. In other words, energy dissipation in dry sands is principally through rotation and gains momentum with increasing motion frequency from 3 to 5 Hz. In Fig. 8, saturated sand exhibits a larger cumulative plastic settlement. In other words, energy dissipation in saturated sands is principally through settlement, particularly under heavier masses, and loses momentum with increasing motion frequency from 3 to 5 Hz.

Displacements

Fig. 8 illustrates the vertical displacements of the foundation. As one would expect, nearly dry sand develops relatively greater values of elastic settlement, whereas saturated sand develops relatively greater values of plastic (and cumulative) settlement. The latter is consistent with observations made in Fig. 7 and in the context of total kinetic energy, where the predominant mode of energy dissipation in saturated sands was established to be through plastic settlement.

The input motion frequency (within the limits of testing 3 and 5 Hz) is inversely related to both elastic and plastic settlement. However, this relationship is more pronounced in subgrade soils under sufficiently high surcharge loads.

The uplift movement of foundations in the form of ground heave is limited to lower 3 Hz loading frequency and early stages of cyclic loading; that early uplift is particularly notable in dry sands. This observation is consistent with earlier discussions, where large rotational movements of the foundation under the testing 3 Hz frequency motion were associated with uplift movements in dry sands.

In Fig. 8(f), a conceptual model of nearly dry sands subjected to shaking is presented. Capillary action causes water to move upward through the soil pores due to surface tension. During seismic excitation, sand particles compress and expand cyclically, leading to water being drawn upward through capillary action. This results in an increase in pore water pressure near the foundation base, a decrease in effective stress, and a reduction in the sand's ability to resist uplift forces. The combination of higher pore water pressure and lower effective stress facilitates the uplift movement of the foundation in the early stages of motion, leading to rotation and rocking movements.

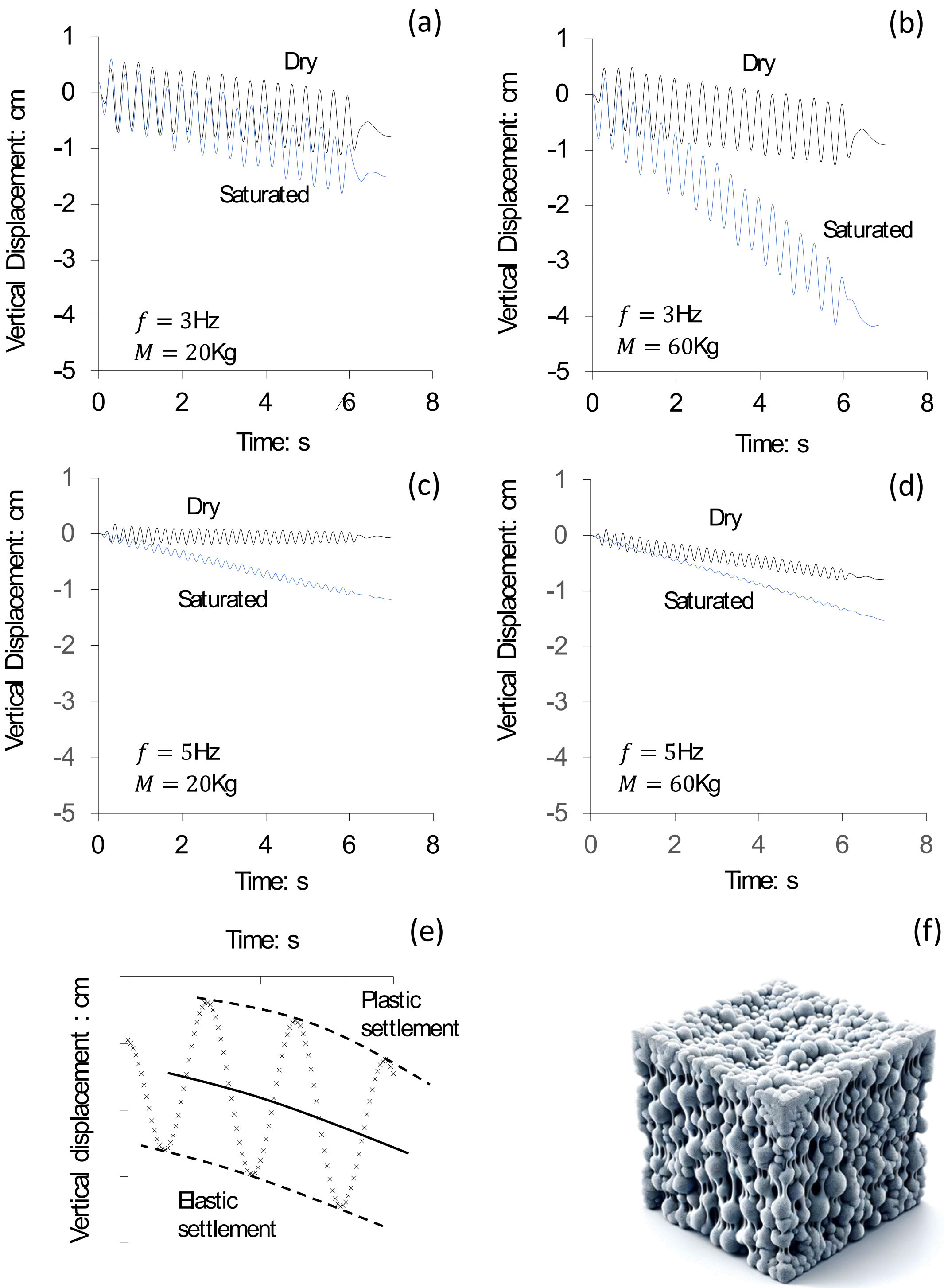

Fig. 8. Vertical displacements: (a) subgrade soil beneath light structure subjected to 3 Hz motion, (b) subgrade soil beneath heavy structure subjected to 3 Hz motion, (c) subgrade soil beneath light structure subjected to 5 Hz motion, (d) subgrade soil beneath heavy structure subjected to 3 Hz motion, (e) concept of elastic and plastic settlements, (f) conceptual model of capillary action and heave in nearly dry sand

Possible Limitations

As noted, in the provision of target relative density, a small amount of water was mixed with dry sand ahead of compaction. In this, the dry sand in this study is in effect a nearly dry sand, despite it being fair to assume, that large proportions of that small added water would have evaporated ahead of the applied seismic motion. The existence of small amounts of water in dry sand merits some elaborations on possible implications. The cumulative foundation rotations and settlements reported here for the nearly dry sand were likely to be slightly larger, had the sand been completely dry. Note that the rotational energy dissipation at the surface is through two coinciding kinetic rotational and kinetic translational mechanisms. Thereby it is hard to say what would have been the effect on the rotational energy dissipation had the sand been completely dry. Cautiously put, rotational energy dissipation at the surface is likely to be modestly lower, have the sand been completely dry. The smaller rotations, in the presence of matric suction, albeit little, are due to enhanced stiffness and strength.

Rotational Stiffness and Damping

In the context of soil dynamics, rotational stiffness (K_r) refers to the resistance provided by a soil-structure system to rotation under the influence of applied moments or forces. It characterises the soil's ability to deform and rotate in response to external loads. Mathematically, K_r represents the rate at which the moment is changing concerning rotation.

The damping ratio (ξ) characterizes the level of damping or energy dissipation in a soil-structure system subjected to dynamic loads or cyclic loading. It describes how rapidly oscillations in the system decay over time. A higher damping ratio indicates more significant dissipation and quicker decay of vibrations.

Methods followed in Sharma and Deng [29] are adopted here. The rotational stiffness can be represented by the slope of the line that passes through the opposite ends of the hysteresis loop on the $M - \theta$ diagram. This is demonstrated in Equation 2.

$$K_{sec} = \frac{M_{(\theta_{max})}}{\theta_{max}} \tag{2}$$

However, the maximum moment (M_{max}) does not necessarily coincide with the maximum footing rotation (θ_{max}). Therefore, the ratio of the maximum moment in each cycle to the maximum recorded rotation in that cycle may provide a more accurate representation of rotational stiffness (see Equation 3). During cyclic loading, the contact surface between the footing and the subsoil may alter at any moment due to the footing's rocking motion, resulting in either an increase or a decrease in the contact area. Any change in the contact surface leads to a corresponding adjustment in the system's rotational stiffness. To this end, the secant stiffness is,

$$K_{sec} = \frac{M_{max}}{\theta_{max}} \tag{3}$$

In Figs. 9(a)-(b), the stiffness is normalised by the initial stiffness, which is the slope of the linear portion of the $M - \theta$ curve.

The damping ratio is calculated via a simple MATLAB code, and by dividing the area enclosed by each $M - \theta$ hysteresis loop by four times π times the area of a triangle. This triangle has a height of M_{max} and a base of θ_{max}. The formula is expressed as,

$$\xi = \frac{\Delta E_{cycle}}{4\pi \Delta E_{el}} \tag{4}$$

where ΔE_{cycle} is the area enclosed by a specific hysteresis loop and ΔE_{el} is the area of a triangle defined by the coordinates (0,0), (0, θ_{max}), and (M_{max}, θ_{max}).

Figure 9(a) and (b) demonstrate the evolution of normalised rotation stiffness with loading cycles for the lightest and the heaviest structures, for the $f = 5$ Hz motion. Immediate inspection shows that the normalised rotational stiffness decreases with loading cycles and increases with mass of structure. The degradation is non-linear. Turner et al. [25] reported similar non-linearity and attributed that to soil rounding beneath the foundation. The direct relationship between normalised stiffness and mass marks a restriction on the rocking motion for heavy structures. The lower foundation rotation angles (θ_f) in Fig. 7 for heavier structures correspond well with the observations here. It also evident that the dependency of rotational stiffness on mass becomes more marked in saturated sands.

Figures 9(c) to 9(f) demonstrate the variation of damping with loading cycles for the lightest and heaviest structures subjected to the $f = 3$ Hz and $f = 5$ Hz motions.

The damping ratio generally decreases with loading cycles. In other words, cyclic loading appears to compromise the soil structure. Observations here are consistent with findings of Khosravi et al. [5], Turner et al. [25] and Allmond [30] for sands at various saturation states. To explain the concurrent degradation of damping and rotational stiffness, two mechanisms can be identified: (i) Due to cyclic loading, particles rearrange, and the packing becomes denser. As particles draw closer together, the coordination number increases [31], leading to a rise in inter-particle contact points. This change facilitates a more uniform distribution of skeletal stresses, resulting in a decrease in energy absorption per cycle. (ii) In saturated sands, excess pore pressures lead to softening and a partial loss of the soil's capacity to dissipate energy through damping.

It is interesting to see the consistency of equivalent damping ratio for saturated sand with those of clay (0.08-0.3) in Sharma and Deng [16], up to 0.4 in Sharma and Deng [17], and viscous damping of 0.10-0.35 in Sharma and Deng [29]. When comparing the data, reader should note that, the horizontal axis in Fig. 9 reads the number of input cycles and that may differ from seemingly similar diagrams in the literature. In the context of pore water, viscous damping is relatively higher in saturated sands and is powered by flow of pore water through the pore network.

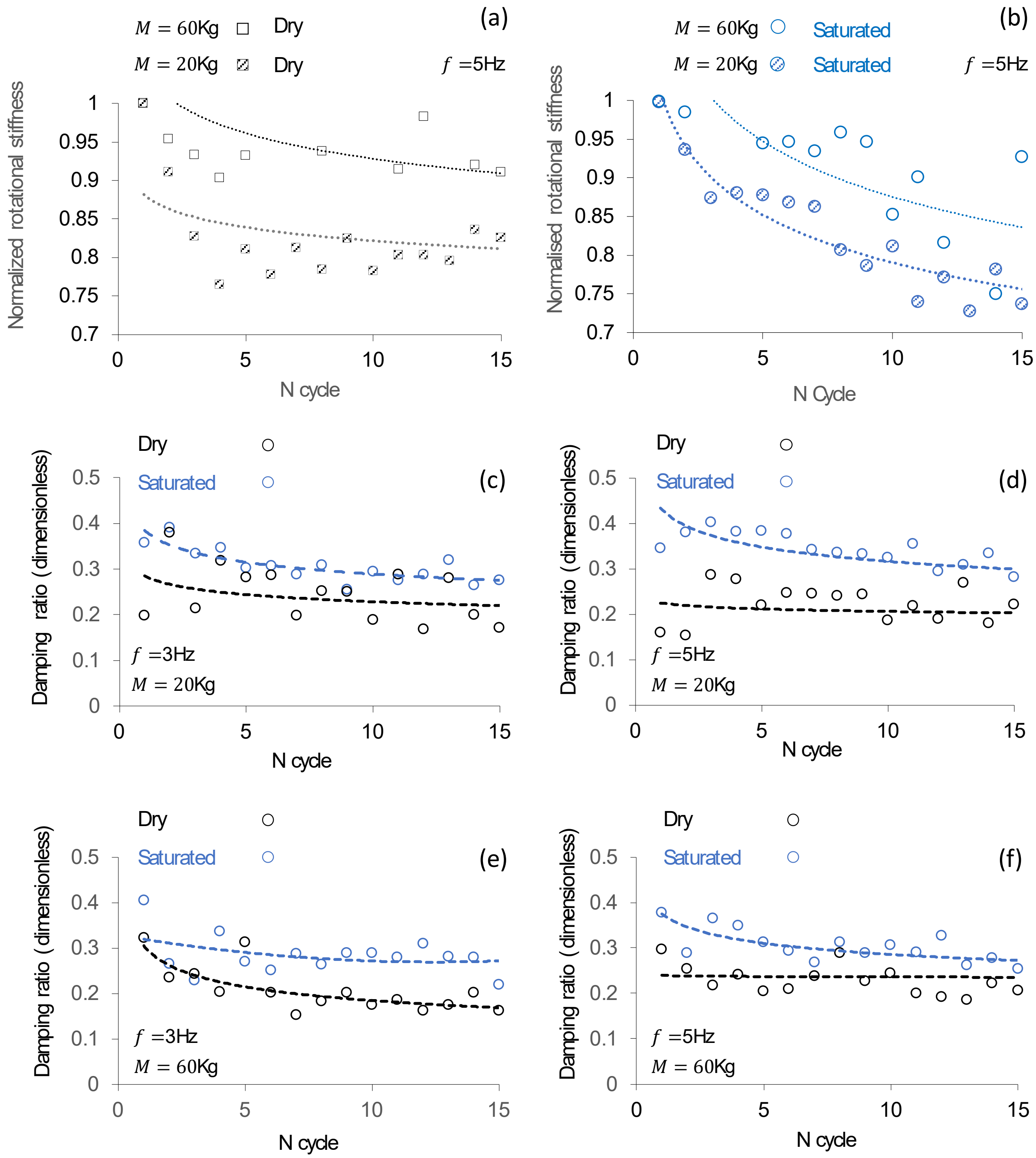

440

441 **Fig. 9.** Normalised rotational stiffness and damping versus loading cycles

442 **Free Decay Response**

To better identify the nonlinearity and rocking performance of testing systems, it is vital to measure and capture the variation with time of fundamental period ($T_{n,i}$) and damping ratio (ξ_i), and the associated system's acceleration response amplitudes. Time here refers to post-vibration conditions, through which the acceleration decays. Of seminal works that address the damping of shallow foundations subjected to rocking oscillations are Tomassetti et al. [32], Spanos et al. [33], Adamidis et al. [34], Wiebe et al. [35], Anastasopoulos et al. [36], and Makris and Konstantinidis [37]. Most recently, de Silva et al. [38] correlated the nonlinear variation of the foundation stiffness and damping ratio with the increasing amplitude of the foundation translation and rocking motions (θ_{fmax}) and proposed sets of empirical equations. To this end, for two concentrated masses of 20 and 60 Kg and higher motion frequency of 5 Hz, the procedures proposed in Arabpanahan et al. [39], and Kashani et al. [40-41] were followed to determine the frequency at time instant ($f_{n,i} = 1/t_{i+1} - t_i$). The t_i is the time instant i and the $t_{i+1} - t_i$ is the period, $T_{n,i}$. The procedure was also utilised to determine the damping ratio at time instant i — that is ξ_i. The procedure is based on the free decay vibration, when the input motion stops, and system freely vibrates to return to static conditions and behaviour transitions from nonlinear to linear. Free decay motion can be seen in the acceleration time history in Fig. 10(a). The motion amplitude subsides during the free decay due to damping. The procedure constituted five steps. The free decay response was trimmed at both ends through removing the static components. The acceleration response's low-magnitude, high-frequency components were eliminated using a zero-phase fourth-order low-pass Butterworth filter, which has a cut-off frequency of 10 Hz. Zero-phase filtering ensures that there is no time shift in the filtered signal. The amplitude at time instant t_i (for the i^{th} vibration) was then determined ($A_{c,i}$). This led to the determination of the frequency and period at time instant t_i ($f_{n,i}$ and $T_{n,i}$). An exponential curve was then fitted to $A_{c,i}$ and $A_{c,i+1}$ — corresponding to time instants t_i and t_{i+1}, to determine the damping ratio, ξ_i. The latter procedure is demonstrated in Fig. 10(b) and Equation 5. In Figure. 10(b), to ascertain the instantaneous damping ratio (ξ_i), an exponential curve is fitted to X_{ci} and X_{ci+1} at time instances t_i and t_{i+1}, respectively.

$$\log_e \frac{x_A}{x_B} = \frac{2\pi\xi_i}{\sqrt{1-\xi_i^{\,2}}} \tag{5}$$

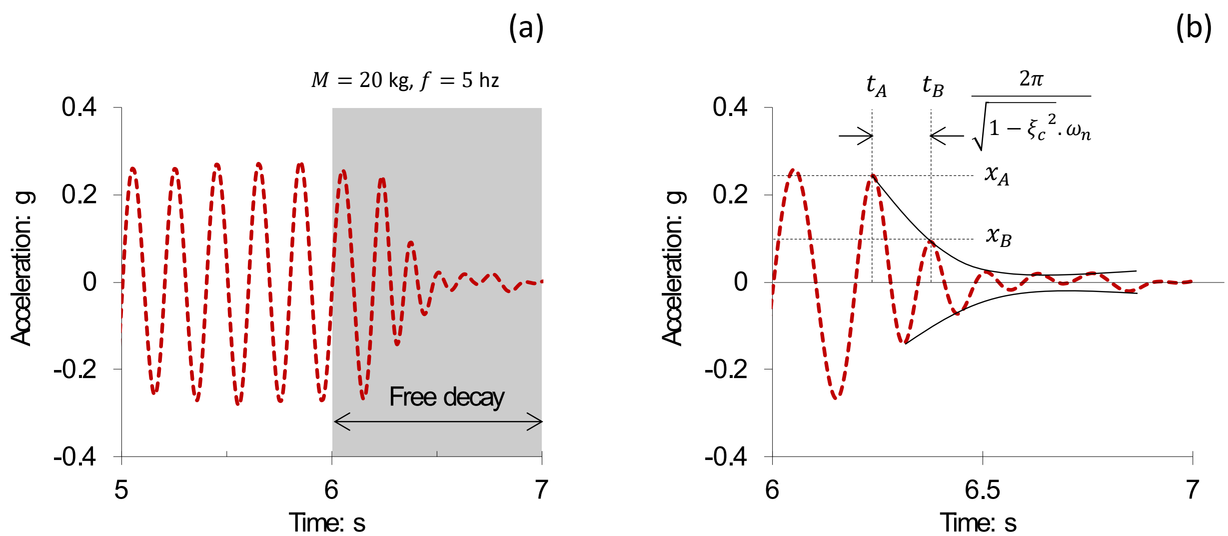

Fig. 10. (a) free decay motion on Acceleration response time history, (b) damping ratio (ξ_i) at time instant t_i

Points A and B in Equation 5 stand for two consecutive peaks on an underdamped system's response curve. In the time instance of t_A and t_B, respectively, x_A and x_B denote the amplitude corresponding to points A and B, respectively.

Figure 11 demonstrates the free decay response for the lightest ($M = 20$ Kg) and heaviest ($M = 60$ kg) structures. The frequency at time instant t_i ($f_{n,i}$) increased with time and as the amplitude dropped progressively. The rise in frequency can be attributed to the decrease in rotation, re-establishment of soil-structure contact and stiffness. Mass is directly correlated with the $f_{n,i}$, indicating the more marked nonlinearity of soil behaviour under heavier structure.

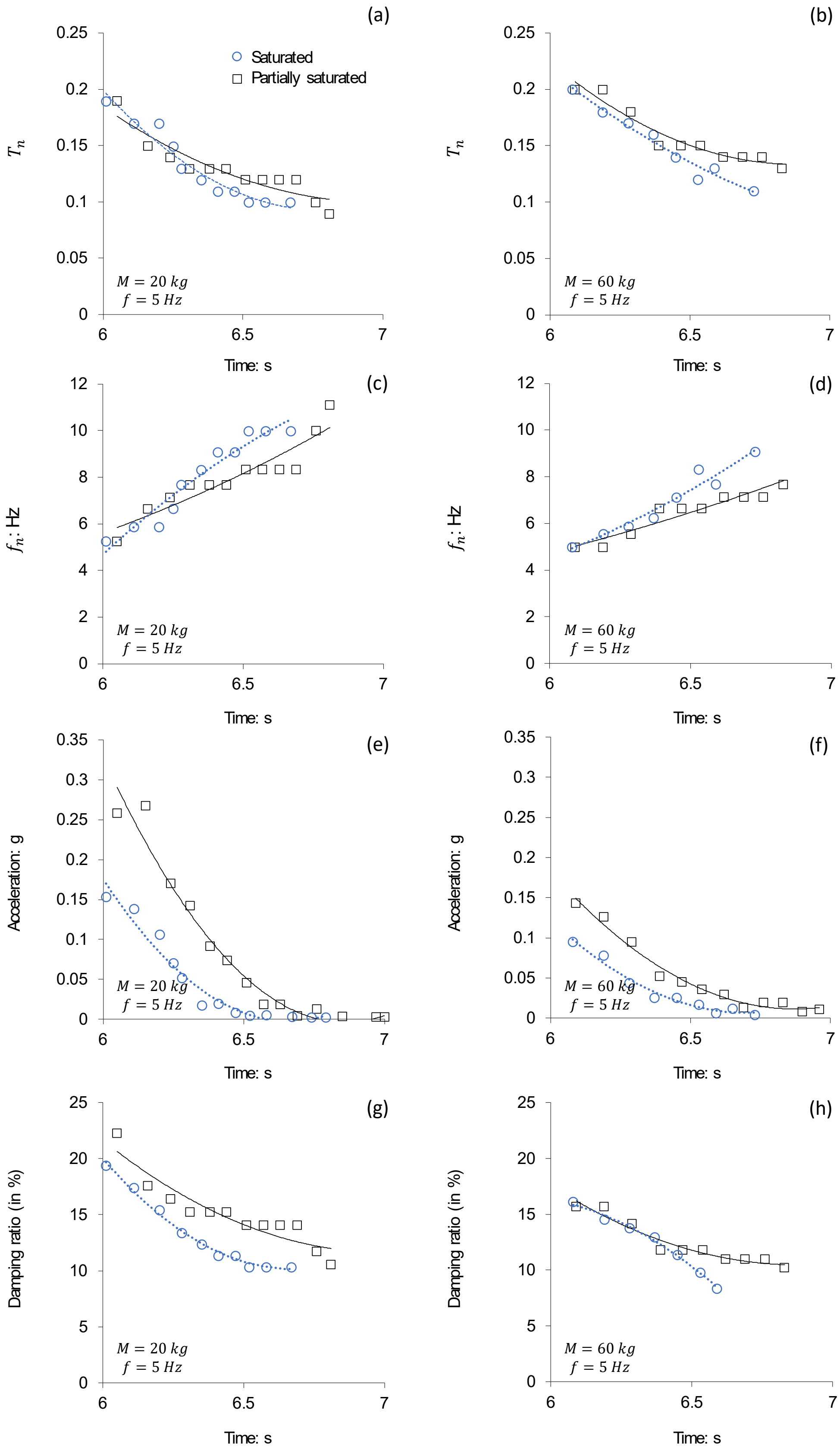
(a)
(b)
(c)
(d)
(e)
(f)
(g)
(h)
Saturated
Partially saturated
T_n
f_n: Hz
Acceleration: g
Damping ratio (in %)
Time: s
$M = 20\ kg$
$f = 5\ Hz$
$M = 60\ kg$
$f = 5\ Hz$

Fig. 11. The motion decay for input 5 Hz sinusoidal motion, (a)-(b) period at varied time instances, (c)-(d) frequency at varied time instances, (e)-(f) filtered and trimmed acceleration response, (g)-(h) damping ratio at varied time instances.

For both dry and saturated sands, an increase in decay time (and hence decreasing acceleration amplitude) led to decreasing period (T_n) and reciprocal increase in frequency ($f_{n,i}$) at time instant t_i — see Fig. 11(a)-(d). This is consistent with earlier observations of Irani et al. [41-42] and indicative of foundation re-centring as the contact surface between soil and foundation re-establishes. The change in frequency with time is relatively faster in the case of saturated sands, indicating the impacts and contribution of evolving pore water pressures. Saturated sands experience relatively lower damping ratios at any given post-motion time.

CONCLUSIONS

Rocking foundation incorporates weakening of footing and compromising the foundation moment capacity, so to transform the foundation into a 'fuse' to avoid plastic hinges forming in the column. This study examines the rocking foundation on a fine, medium-dense sand beneath a range of lightweight masses and explores the inter-playing of mass, motion frequency, and degree of saturation. A single-degree-of-freedom, mid-rise lightweight prototype deck mass-column-footing model is built on sand and subjected to sinusoidal shaking.

Findings here are constrained to two testing input motions of 3 and 5 Hz frequency, and the F161 well-sorted, fine, sub-angular sand (similar to Ottawa C109 in shape and size) compacted to a relative density of just above 70% in two fully saturated and nearly dry states.

In the case of saturated sand,

1. Lower peak accelerations and amplification beneath and above the structure, alongside decentralised and wide $M - \theta$ loops, suggest greater energy dissipation.
2. The principal mechanism of energy dissipation is plastic settlement, especially under heavier loads.
3. Negative pore water pressures, peaking beneath the foundation's edge, maintain amplitude throughout the motion, indicative of a breakaway gap with sustained porosity.
4. Rapid changes in pore pressures beneath the foundation's edge indicates the breakaway gap's role in facilitating rocking motions.
5. Water efflux towards dissipating excess pore water pressure, results in significant plastic settlements once the motion ceases.
6. Foundation recentring appears easier under relatively lighter structures, evidenced by more frequent changes in pore pressures beneath the foundation edge, a wider range of footing rotation angles, and larger amplifications above the lighter structure.

In the case of nearly dry sand,

1. The $M - \theta$ loops close with increasing surcharge, indicating decreased energy dissipation as surcharge increases.
2. Energy dissipation primarily occurs through rotation.
3. Notable foundations uplift at the early stages of motion is consistent with large rotational movements.

For all testing sands,

1. The normalised rotational stiffness and damping degrade nonlinearly across loading cycles, possibly due to particle rearrangement and more uniform distribution of skeletal stresses.
2. During the free decay phase, both the period (T_n) and amplitude decrease, leading to progressive increase in frequency at time instant t_i ($f_{n,i}$). These changes are more pronounced in saturated sands and suggest foundation recentring as the contact surface between soil and foundation re-establishes.

REFERENCES

1. Stewart, J. P., Kim, S., Bielak, J., Dobry, R., & Power, M. S. (2003). Revisions to Soil-Structure Interaction Procedures in NEHRP Design Provisions. In Earthquake Spectra (Vol. 19, Issue 3). https://doi.org/10.1193/1.1596213
2. Anon. (2000). Minimum design loads for buildings and other structures. In ANSI/ASCE Standard (Issue 7 98). https://doi.org/10.1061/9780872629042
3. Hung, H. H., Liu, K. Y., Ho, T. H., & Chang, K. C. (2011). An experimental study on the rocking response of bridge piers with spread footing foundations. Earthquake Engineering and Structural Dynamics, 40(7). https://doi.org/10.1002/eqe.1057\
4. Figini, R., & Paolucci, R. (2017). Integrated foundation–structure seismic assessment through non-linear dynamic analyses. Earthquake Engineering and Structural Dynamics, 46(3). https://doi.org/10.1002/eqe.2790
5. Khosravi, A., Stuedlein, A. W., & Higgins, C. (2021). New Formulation for Estimating the Moment Capacity of Rocking Shallow Foundations Resting on Partially Saturated Soil. Journal of Bridge Engineering, 26(11). https://doi.org/10.1061/(asce)be.1943-5592.0001783
6. Housner, G. W. (1963). The behavior of inverted pendulum structures during earthquakes. Bulletin of the Seismological Society of America, 53(2). https://doi.org/10.1785/bssa0530020403
7. Gajan, S., Kutter, B. L., Phalen, J. D., Hutchinson, T. C., & Martin, G. R. (2005). Centrifuge modeling of load-deformation behavior of rocking shallow foundations. Soil Dynamics and Earthquake Engineering, 25(7–10). https://doi.org/10.1016/j.soildyn.2004.11.019

8. Sharma, K., & Bin, J. (2022) Introduction to a performance-based design method for rocking shallow foundations in seismic zone. The 75th Canadian Geotechnical Conference, GeoCalgary 2022, Reflection on Resources.
9. Priestley, M. J. N., Seible, F., & Calvi, G. M. (1996). Seismic Design and Retrofit of Bridges. In Seismic Design and Retrofit of Bridges. https://doi.org/10.1002/9780470172858
10. Liu, W., & Hutchinson, T. C. (2018). Numerical investigation of stone columns as a method for improving the performance of rocking foundation systems. Soil Dynamics and Earthquake Engineering, 106. https://doi.org/10.1016/j.soildyn.2017.10.015
11. Gajan, S., & Kutter, B. L. (2008). Capacity, Settlement, and Energy Dissipation of Shallow Footings Subjected to Rocking. Journal of Geotechnical and Geoenvironmental Engineering, 134(8). https://doi.org/10.1061/(asce)1090-0241(2008)134:8(1129)
12. Terzaghi, K. (1943). Theoretical Soil Mechanics. In Theoretical Soil Mechanics. https://doi.org/10.1002/9780470172766
13. Taeseri, D., Laue, J., & Anastasopoulos, I. (2019). Non-linear rocking stiffness of embedded foundations in sand. Géotechnique, 69(9). https://doi.org/10.1680/jgeot.17.P.201
14. Allmond, J. and Kutter, B.L., 2012. Centrifuge testing of rocking foundations on saturated and submerged sand: Centrifuge Data Report for JDA01. University of California at Davis Center for Geotechnical Modeling Report No. UCD/CGMDR-12/01, Davis, CA.
15. Hakhamaneshi., M. (2014). Rocking foundations for building systems, effect of footing shape, soil environment, embedment and normalized moment-to-shear ratio, PhD thesis, University of California, Davis, CA, USA.
16. Sharma, K. & Deng, L. (2019). Characterization of rocking shallow foundations on cohesive soil using field snap-back tests. *Journal of Geotechnical and Geoenvironmental Engineering*, *145*(9), p.04019058.
17. Sharma, K. & Deng, L. (2020). Field testing of rocking foundations in cohesive soil: cyclic performance and footing mechanical response. *Canadian Geotechnical Journal*, *57*(6), pp.828-839.
18. Shirato, M., Kouno, T., Asai, R., Nakatani, S., Fukui, J. & Paolucci, R. (2008). Large-scale experiments on nonlinear behavior of shallow foundations subjected to strong earthquakes. *Soils and foundations*, *48*(5), pp.673-692.
19. Tsatsis, A. and Anastasopoulos, I., 2015. Performance of rocking systems on shallow improved sand: shaking table testing. *Frontiers in Built Environment*, *1*, p.9.
20. Gavras, A.G., Kutter, B.L., Hakhamaneshi, M., Gajan, S., Tsatsis, A., Sharma, K., Kohno, T., Deng, L., Anastasopoulos, I. and Gazetas, G., 2020. Database of rocking shallow foundation performance: Dynamic shaking. *Earthquake Spectra*, *36*(2), pp.960-982.

21. Allmond, J.D. and Kutter, B.L., 2014. Design considerations for rocking foundations on unattached piles. *Journal of Geotechnical and Geoenvironmental Engineering*, *140*(10), p.04014058.
22. Takahashi, A., Omura, N., Kobayashi, T., Kamata, Y. and Inagaki, S., 2022. Centrifuge model tests on large-diameter monopiles in dense sand subjected to two-way lateral cyclic loading in short-term. *Soils and Foundations*, *62*(3), p.101148.
23. Hakhamaneshi, M., & Kutter, B. L. (2016). Effect of Footing Shape and Embedment on the Settlement, Recentering, and Energy Dissipation of Shallow Footings Subjected to Rocking. Journal of Geotechnical and Geoenvironmental Engineering, 142(12). https://doi.org/10.1061/(asce)gt.1943-5606.0001564
24. Burland, J. B., & Burbidge, M. C. (1985). Settlement of foundations on sand and gravel. Proceedings of the Institution of Civil Engineers (London), 78(pt 1). https://doi.org/10.1680/iicep.1985.1058
25. Turner, M. M., Ghayoomi, M., Ueda, K., & Uzuoka, R. (2022). Performance of rocking foundations on unsaturated soil layers with variable groundwater levels. Géotechnique, 72(11). https://doi.org/10.1680/jgeot.20.P.221
26. Deng, L., & Kutter, B. L. (2012). Characterization of rocking shallow foundations using centrifuge model tests. Earthquake Engineering and Structural Dynamics, 41(5). https://doi.org/10.1002/eqe.1181
27. Hansen, J. B. (1970). A Revised and Extended Formula for Bearing Capacity. Bulletin of the Danish Geotechnical Institute, 28(28).
28. Antonellis, G., Gavras, A. G., Panagiotou, M., Kutter, B. L., Guerrini, G., Sander, A. C., & Fox, P. J. (2015). Shake Table Test of Large-Scale Bridge Columns Supported on Rocking Shallow Foundations. Journal of Geotechnical and Geoenvironmental Engineering, 141(5). https://doi.org/10.1061/(asce)gt.1943-5606.0001284
29. Sharma, K. and Deng, L. (2021) Effects of loading obliquity on field performance of rocking shallow foundations in cohesive soil. Géotechnique, 71(4), pp.320-333.
30. Allmond, Jacquelyn Denise. *Shallow rocking foundations in liquefiable and saturated soil conditions*. University of California, Davis, 2014.
31. Assadi-Langroudi, A. and Jefferson, I. (2016) The response of reworked aerosols to climate through estimation of inter-particle forces. International journal of environmental science and technology, 13, pp.1159-1168.
32. Tomassetti, U., Graziotti, F., Sorrentino, L. and Penna, A. (2019). Modelling rocking response via equivalent viscous damping. Earthquake Engineering & Structural Dynamics, 48(11), pp.1277-1296.
33. Spanos, P.D., Di Matteo, A., Pirrotta, A. and Di Paola, M. (2017). Nonlinear rocking of rigid blocks on flexible foundation: analysis and experiments. Procedia engineering, 199, pp.284-289.

34. Adamidis, O., Gazetas, G., Anastasopoulos, I. and Argyrou, C. (2014). Equivalent-linear stiffness and damping in rocking of circular and strip foundations. Bulletin of Earthquake Engineering, 12(3), pp.1177-1200.
35. Wiebe, L., Christopoulos, C., Tremblay, R. and Leclerc, M. (2012). Modelling inherent damping for rocking systems: results of large-scale shake table testing. In Proceedings of the 15th World Conference on Earthquake Engineering (pp. 24-28).
36. Anastasopoulos, I., Loli, M., Georgarakos, T. and Drosos, V. (2013). Shaking table testing of rocking—isolated bridge pier on sand. Journal of Earthquake Engineering, 17(1), pp.1-32.
37. Makris, N. and Konstantinidis, D. (2003). The rocking spectrum and the limitations of practical design methodologies. Earthquake engineering & structural dynamics, 32(2), pp.265-289.
38. de Silva, F., Amendola, C., Pitilakis, D. and Silvestri, F. (2023). Prediction of foundation stiffness and damping ratio under horizontal translation and rocking motion. Soil Dynamics and Earthquake Engineering, 166, p.107735.
39. Arabpanahan, M., Mirghaderi, S. R., Hosseini, A. & Ghalandarzadeh, A. (2021). Dynamic rocking response of SDOF-embedded foundation systems using shake table experiments. Soil Dynamics and Earthquake Engineering, 140, p.106431. https://doi.org/10.1016/j.soildyn.2020.106431
40. Kashani, M. M., Ahmadi, E., Gonzalez-Buelga, A., Zhang, D. & Scarpa, F. (2019). Layered composite entangled wire materials blocks as pre-tensioned vertebral rocking columns. Composite Structures, 214,153-163. https://doi.org/10.1016/j.compstruct.2019.02.021
41. Kashani, M. M., Ge, X., Dietz, M. S., Crewe, A. J. & Alexander, N. A. (2019). Significance of non-stationary characteristics of ground-motion on structural damage: shaking table study. Bulletin of Earthquake Engineering, 17, 4885-4907. https://doi.org/10.1007/s10518-019-00668-3
42. Irani, A. E., Bonab, M. H., Sarand, F. B., & Katebi, H. (2023). Overall Improvement of Seismic Resilience by Rocking Foundation and Trade-off Implications. International Journal of Geosynthetics and Ground Engineering, 9(4), 40. https://doi.org/10.1007/s40891-023-00454-x
43. Irani, A. E., Bonab, M. H., Sarand, F. B., & Katebi, H. (2023). Investigation on the behavior of bridge piers considering rocking isolation constructed on non-plastic silts and sands using 1g shaking table tests. Periodica Polytechnica Civil Engineering, 67(3), 835-845. https://doi.org/10.3311/PPci.21713

AUTHOR STATEMENT

Esmatkhah Irani, A. came up with the concepts, designed the methods, fabricated the test setup, conducted experiments and analysis, and wrote the first draft. **Hajialilue-Bonab, M** came up with concepts, supervised the entire project, and had major inputs during the revision round. **Assadi-Langroudi, A.** conducted supplementary analysis, wrote the second draft, edited the artworks, also the final copy. **Maleki Tabrizi** contributed to visualization, instrumentation, editing, and data management.

ACKNOWLEDGEMENTS

The authors acknowledge the support of technicians and support staff at the University of Tabriz. The project did not receive any external funding.